Structural determination of neutral Co_n clusters (n = 4–10,13) through IR-UV two-color vibrational spectroscopy and DFT calculations.

J. M. Bakker,[1, a)] J. Jalink,[2] D. Dieleman,[2] and A. Kirilyuk[3, b)]

[1)] *Radboud University, Institute for Molecules and Materials, FELIX Laboratory, Toernooiveld 7c, 6525 ED Nijmegen, Netherlands*

[2)] *Radboud University, Institute for Molecules and Materials, Heyendaalseweg 135, 6525 AJ Nijmegen, Netherlands*

[3)] *Radboud University, Institute for Molecules and Materials, FELIX Laboratory, Toernooiveld 7c, 6525 ED Nijmegen, Netherlands*

We recorded IR spectra for neutral cobalt clusters *via* two-color IR-UV ionization, using the Free Electron Laser for IntraCavity Experiments (FELICE). Well-resolved IR spectra are presented for Co_n (n = 4–10, 13) and analyzed with the help of Density Functional Theory calculations using two different correlation exchange functionals: the revisited Tao-Perdew-Staroverov-Scuseria (revTPSS) and the frequently used Perdew-Burke-Ernzerhof (PBE) approaches. Although we have not performed an extensive structure search, we tentatively assign the spectra for all cluster sizes except for $n = 7$, and $n = 10$. We find that neither of the two functionals chosen clearly outperforms the other in predicting IR spectra, and that relatively low scaling factors of 0.82 (PBE) and 0.8 (revTPSS) are required. In contrast to the magnetic moments, the calculated electric dipole moments fluctuate strongly as a function of cluster size and could therefore be used as an indirect probe to the cluster structure.

[a)]Electronic mail: j.bakker@ru.nl

[b)]Electronic mail: a.kirilyuk@science.ru.nl

I. INTRODUCTION

Nanostructures can be used as model systems to gain a deeper understanding in condensed matter physics and are required to continue the ongoing technological miniaturization[1,2]. A special class of nanostructures are clusters, containing from 2 up to several hundreds of atoms. Cluster properties evolve in often unexpected ways as a function of size, something which can be revealed when studying them isolated in the gas-phase[3–5]. Neutral clusters of $3d$ transition metal elements, for example, exhibit a strongly size-dependent magnetic moment[6–11]. Moreover, a marked increase in magnetic moment per atom as compared to the bulk value is observed, which can in part be explained by the reduced hybridization of $3d$ and $4s$ orbitals and is a topic of many computational studies[12–18]. A recent spur of experiments has addressed the disentanglement of spin and angular magnetic moments in size-selected cationic 3d metal clusters through X-ray Magnetic Circular Dichroism (XMCD) spectroscopy[19–23]. Here, it was found that cationic cobalt clusters exhibit strong increase in orbital contribution with reduced cluster size[19].

3d transition metal clusters are not only interesting for their magnetic character, but also can act as catalysts. The production of hydrocarbons in the Fischer–Tropsch process, for instance, is catalyzed by cobalt in nanoparticle form.[24,25] The catalytic activity was predicted by Density Functional Theory (DFT) calculations to strongly depend on cobalt particle size[24], using both face centered cubic and icosahedral structures; the size-dependent activity was also found experimentally.[26] As the carbon monoxide binding energy to cobalt depends on, inter alia, the structure,[27,28] an understanding of these materials at the nanoscale is of both fundamental and technological importance.

In this contribution, we focus on the structure of neutral cobalt clusters. Obtaining definitive information on the geometrical arrangement of the atoms in such small systems is a challenge both experimentally and computationally. Several computational studies report icosahedral structures for neutral cobalt clusters[15,16], while Datta *et al.*[17] finds hexagonal geometries. More recently, star-like icosahedral structures are suggested for intermediate-sized cobalt clusters[29]. There is no consensus for the structure of small cobalt clusters either. For example, Co_4 is either found to adopt tetrahedral[15,17], rhombic[16,30] or out-of-plane rhombic[18] symmetry. Similarly, Co_5 can be a bicapped triangle[15,17], planar W-like[30] or a tetragonal pyramid[16]. Clearly, an experimental probe of the cluster structure is required

to solve this problem.

A variety of experimental techniques has been developed to obtain direct structural information. Among these are chemical probe methods[31], trapped ion electron diffraction[32] and IR vibrational spectroscopy[33]. Cobalt anions were investigated using photoelectron spectroscopy[34], comparing the experimental photoelectron spectra to calculations[35]. IR spectroscopic information was obtained for cationic cobalt clusters ranging from Co_4^+ to Co_8^+ through IR-multiple photon dissociation (IR-MPD) spectroscopy of Co_n^+-Ar complexes[36]. However, the formation of such weakly bound complexes for neutral cobalt clusters, enabling messenger spectroscopy, has not been reported thus far.

The IR absorption characteristics of *neutral* clusters can also be probed using an IR-UV two-photon ionization technique. Here, a UV laser that is slightly red-detuned from the ionization wavelength, can succeed in ionizing the cluster once the cluster resonantly absorbs one or multiple IR photons to raise its energy and overcome the ionization barrier. This method has been used for several systems[37–39], most notably for Si, MgO and B clusters[40–42]. We recently demonstrated that the IR excitation of neutral cobalt clusters leads to a thermal equilibration between nuclear and electronic coordinates, and that the functional form of the UV wavelength dependent photoionization signal reveals information about the electronic structure[43]. We showed that the IR excitation is done in resonance with vibrational modes, revealing cluster size dependent UV spectra. In this work, we present the IR spectra recorded for the various cobalt clusters. We combine the IR spectra with DFT calculations using two correlation-exchange functionals revTPSS and PBE to determine the structure of Co_n for n=4–10,13 clusters. Finally, we will discuss the electronic and magnetic properties of the structures.

II. METHODS

A. Experiment

The experiments are carried out in a molecular beam instrument that is coupled to the Free-Electron Laser for IntraCavity Experiments FELICE. Details about this instrument are described elsewhere[44,45], and will only be outlined briefly. A pulsed Nd:YAG laser (532 nm) ablates material from a cobalt sample rod (Goodfellow, high purity 99.99% Co) in the

presence of a pulse of helium gas, introduced to induce cluster condensation. Subsequently, clusters aggregate in a growth channel which is cooled to about 77 K and expand into vacuum via a nozzle to form a molecular beam. The cluster beam is skimmed and enters a differentially pumped vacuum chamber where charged clusters are deflected out of the beam using a set of electrically biased parallel plates. Neutral clusters are transmitted to the extraction region of a reflectron time-of-flight mass spectrometer (Jordan TOF products, Inc.) where they are overlapped by pulsed IR and UV laser beams, under angles of 35° and 90°, respectively. The extraction plates of the mass-spectrometer are continuously on, leading to instantaneous extraction upon the formation of ions, which are detected on a multichannel plate (MCP) detector. The MCP signal is registered by a 12-bit 100 MHz digitizer at 2.5 ns time resolution (Acqiris DP310).

FELICE produces IR light at 10 Hz in macropulses of $\sim$ 7 μs consisting of a pulse train of ps duration micropulses at a 1 GHz repetition rate. FELICE covers the 100-3500 cm^{-1}spectral range, although in this study only the 100-500 cm^{-1}range is used. The spectral bandwidth of the light is set to $\sim$ 0.3% of the central frequency.

The UV laser pulses are produced either by an ArF excimer laser or a frequency-tripled dye laser. Both UV lasers operate at twice the FELICE repetition rate. This way, two types of mass spectra are obtained in an alternating fashion: one with and one without IR excitation. The mass spectrum without IR excitation forms a reference mass-spectrum allowing for the correction for long term fluctuations in cluster production. The UV lasers are timed to obtain a maximum increase in ion yield, approximately at 1 μs after the end of the FELICE macropulse.

The two-color IR-UV spectroscopic technique requires that the UV photon energy is tuned close to the ionization energy (IE) of the cluster[39,43,46]. The IEs for Co_4, Co_5 and Co_6 are not exactly known, but were previously estimated at 6.2 $\pm$ 0.2 eV[47,48]. To access this energy range we use an ArF excimer laser at a fixed energy of 6.42 eV/photon. Larger clusters have a lower IE and are probed using a frequency-tripled dye laser.

The energy deposited into the cluster upon excitation of a vibrational mode is redistributed over both nuclear and electronic degrees of freedom. The redistribution of energy leads to population of vibrationally and electronically excited states.[43] By monitoring the relative change in ion yield as a function of IR frequency a vibrational spectrum is obtained, which can be extracted for multiple cluster sizes simultaneously due to the mass spectro-

scopic analysis of the cluster beam. The spectra are presented as the gain, which is given by $I(\nu)/I_0 - 1$ of ion yields $I(\nu)$ and I_0 with and without IR irradiation at frequency ν, respectively, and are subsequently normalized on the macropulse energy.

III. COMPUTATIONAL

We have performed DFT calculations using the ADF program suite[49–51] to interpret the experimental vibrational spectra. Several cluster geometries are considered, starting with previously obtained candidate structures[15,17], but no broad structure search was carried out. Two exchange correlation functionals are considered: the Perdew-Burke-Ernzerhof (PBE) functional in the generalized gradient approximation (GGA)[52] which is used in many computational studies.[17,29,53]. We also make use of the revisited Tao-Perdew-Staroverov-Scuseria (revTPSS) functional in the meta-generalized gradient approximation (Meta-GGA)[54,55]. The revTPSS functional[55] is a recent revision of the original TPSS functional,[54] with which a better agreement with several experimental studies than with PBE has been reported.[56,57]

For both functionals we use ADF's TZ2P+ Slater type exponential spherical basis set and apply scalar (ZORA) relativistic corrections. The calculations are done for different spin polarizations and no symmetry restrictions are applied during the geometry optimization. After geometry optimization we calculate the harmonic frequencies to ensure that the geometries are true minima, and to compare them to the experimental spectra. We finally calculate the electric dipole moment of the cluster, by integrating the charge density.

In comparing harmonic spectra to experimental spectra, a scaling factor is often needed to correct for the anharmonicity of the vibrational potential.[58] Here we apply an empirical frequency scaling factor of 0.82 for PBE, and 0.8 for revTPSS found by comparison with the well-reproduced experimental spectrum for Co_5, *vide infra*. The zero-point energy based on scaled harmonic frequencies is included in calculating the energy differences between isomers. Although our experiments are done at 77K (determined by the cooling extension of our source) and the most relevant quantity for comparison would be a finite-temperature vibrational spectrum calculated using *e.g.* vibrational perturbation theory (VPT2),[59] it has been demonstrated in many experiments that the zero temperature vibrational spectra can be sufficiently accurate for structural assignment.[33]

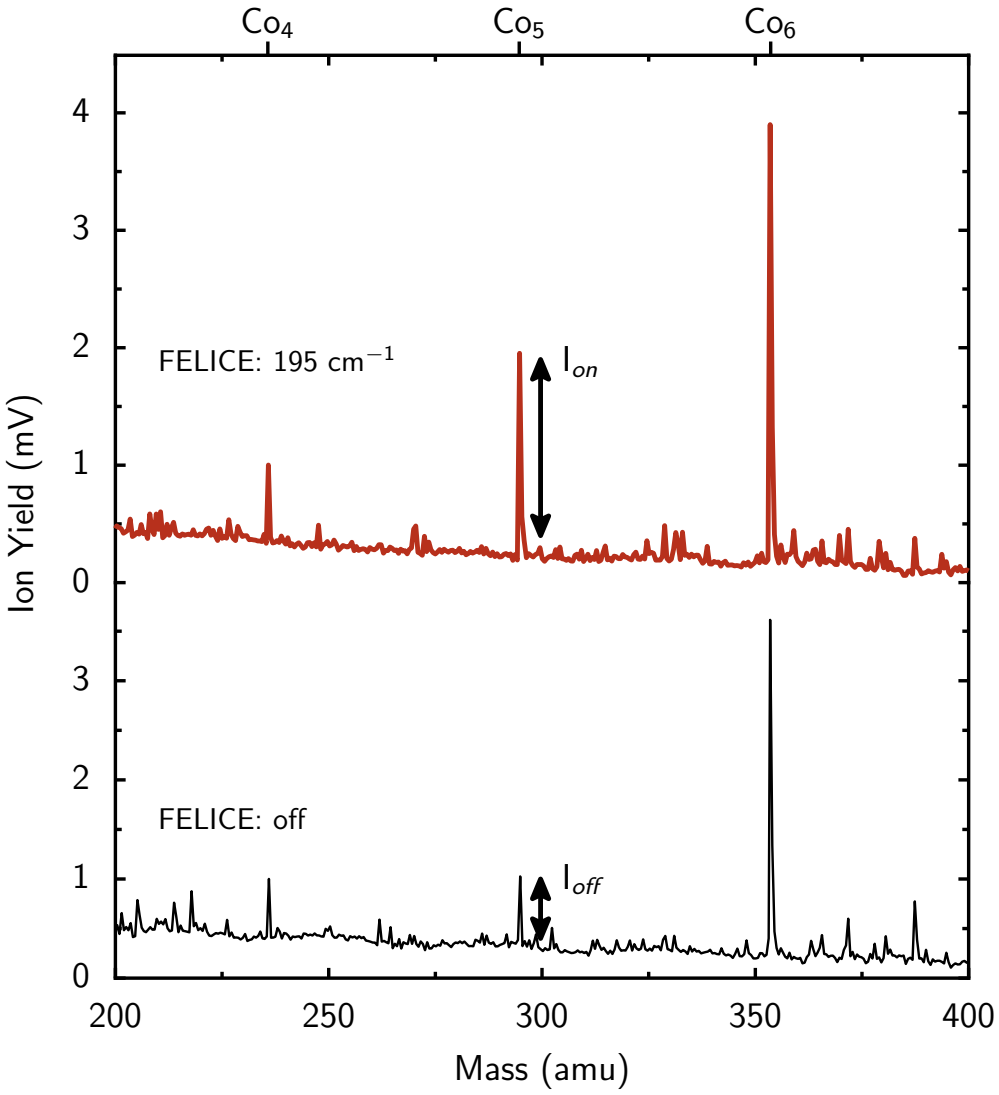

FIG. 1. Mass spectra of cobalt clusters with and without IR excitation at 195 cm^{-1}acquired using a 193 nm ionization laser.

IV. RESULTS AND DISCUSSION

Typical mass spectra in the lower size range show the cluster distribution as detected using photons of 193 nm with and without IR irradiation. (Figure 1). As the photon energy is below the IE for the cobalt clusters shown, and the UV pulse energy is kept low to prevent two-photon ionization, their signal intensities are relatively low, and the mass spectra contain a fair number of dark counts of the MCP detector. Upon IR irradiation at a frequency of 195 cm^{-1}, a clear enhancement of the ion yield is observed for Co_5 compared to the situation without IR laser. Enhancement for Co_4 and Co_6 can also be observed,

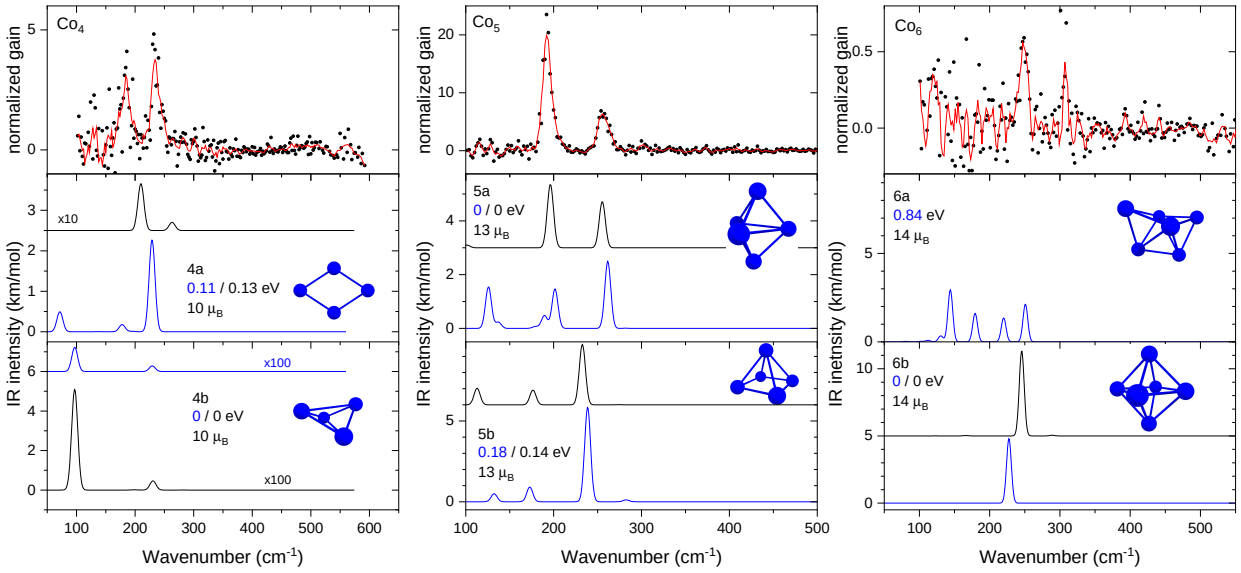

FIG. 2. Experimental vibrational spectra (top panels) for Co_4, Co_5, and Co_6. Bottom panels: calculated spectra for two isomers for each cluster size with relative energies using the PBE (black) and revTPSS (blue) functionals. The calculated IR intensities (in km/mol) are convoluted with Gaussian line shape functions with a 15 cm^{-1} width to facilitate comparison with the experimental spectra.

although to a lesser extent.

By recording this enhancement as a function of IR frequency ν, we have obtained IR spectra for Co_n clusters (n = 4–10,13) by employing a limited number of UV ionization wavelengths. For Co_4–Co_6, which have high IEs, the UV frequency was necessarily fixed by the ArF excimer laser (193 nm, 6.4 eV/photon); for larger clusters, where a tunable laser source is available, time constraints only permitted the use of selected wavelengths. As a result, the signal-to-noise ratio in the experimental spectra can differ from one cluster size to the other, based on how far detuned the laser is from the IE. Although the spectra for, *e.g.*, Co_4 and Co_6 show a poorer signal-to-noise ratio than others, all spectra are relatively well resolved and can serve to, at least tentatively, identify the geometrical structures. All spectra are corrected for the IR macropulse energy, which in the lower frequency region results in a lower signal-to-noise ratio.

In figure 2, experimental gain spectra for Co_4, Co_5, and Co_6 are presented. All are recorded at 193 nm, but the observed gain for Co_5 is clearly substantially larger than for

Co_4 or Co_6. This could be due to larger IR absorption cross sections for Co_5, but the calculations (discussed below) do not substantiate this. Rather, we speculate that the IE for Co_5 is much closer to the photon energy used than that of Co_4, thereby making the probing of repopulated of vibrational and/or electronic states easier. We first discuss the spectra for Co_5 and Co_6 which can readily be assigned to a specific structure, allowing us to motivate the choice for harmonic frequency scaling.

The experimental vibrational spectrum of Co_5 displayed in Figure 2 shows two distinct resonances at 193 and 258 cm^{-1}, respectively. We consider two isomers that were also suggested in previous computational studies for the structure of Co_5[15–17]. Structure **5a** is a D_{3h} trigonal bipyramid, structure **5b** a tetragonal pyramid. While the PBE calculation for **5a** leads to a near-D_{3h} structure, the revTPSS calculations lead to a distorted structure, where the pyramidal axis is slightly off-center. The resulting C_{2v} structure has a markedly different predicted IR spectrum with bands that, while symmetry forbidden in D_{3h}, are allowed with appreciable intensity in C_{2v}. While we have not pursued any calculations, we speculate that the distortion of the revTPSS structure is due to weak Jahn-Teller interactions, and that it is only very little lower in energy than the symmetric structure. Time-averaged, the structure is likely symmetric, an example of the dynamic Jahn-Teller effect, where the zero-point energy is higher than the barrier between the three distorted minima in the potential energy surface, such as previously observed in the benzene cation[60]. Both functionals agree about the relative stability of square pyramidic isomer **5b**, which is found at ~ 0.1 eV higher in energy than the trigonal bipyramid; when frequency scaled with appropriate factors the calculated spectra line up, with most features mirrored. Although the observed intensity ratio of the experimentally found bands at 193 and 456 cm^{-1} is somewhat higher than computationally predicted, the excellent agreement between experimental and calculated vibrational spectra allows us to assign the spectrum to structure **5a** as the ground state structure of Co_5. This is in agreement with previous calculations[15,17]. It is noteworthy that for the cation a similar, however distorted, bipyramid was assigned as the ground state structure[36].

We have chosen frequency scale factors of 0.82 for PBE, and 0.8 for TPSS based on the match for Co_5. We can validate this choice by turning our attention to the spectra for Co_6. For this cluster, there has been a discussion in the literature what the preferred structure is: a capped trigonal bipyramid or boat structure (isomer **6a**) and an octahedron

(**6b**) have been suggested.[15–17,30] The experimental spectrum is rather simple, pointing to a highly symmetric structure. One clear vibrational mode at 249 cm^{-1} (FWHM: 14 cm^{-1}) is observed. (A second feature at 309 cm^{-1} is attributed to experimental noise, as its width (FWHM: 7 cm^{-1}) is substantially below what we observe for other transitions.) In the PBE calculations, the boat structure (**6a**) in the 14 μ_B spin state collapsed into an icosahedron; usingrevTPSS it was found to be an enormous 0.85 eV higher in energy. For other spin isomers, the boat converges, but its energies are consistently higher than the octahedron (Figure S1 and S2). Based on the simplicity of the spectrum, and the match with the single predicted band, we assign the experimental spectrum for Co_6 to the octahedron **6b**. The frequency of the single band predicted matches the experimentally observed band well, confirming the scaling factors chosen. This factor is rather low compared to other scaling factors used, e.g. for PBE calculations for cationic Co_n^+-Ar complexes[36]; we have no clear explanation for this low value for the scaling factor.

In the spectrum for Co_4, two experimental resonances are found at 185 cm^{-1} and at 236 cm^{-1}, with associated widths (FWHM) of 20 and 17 cm^{-1}, respectively. We compare the experimental spectrum to calculated spectra for a tetrahedron and a rhombus. The anion was found to be a slightly distorted tetrahedron with a bond length of 2.25 $\pm$ 0.2 Å[35]. A distorted tetrahedron with D_{2d} symmetry is also found experimentally for the cation[36]. The current calculations using PBE suggest that a tetrahedral structure relaxes into a D_{2d} structure, and is the lowest in energy by 0.1 eV at the PBE level, and 0.3 eV using revTPSS. However, the match between both calculated spectra and the experimental spectrum is not satisfactory, as only a single vibrational band is predicted where two clear bands are observed. This observation is better explained by the rombic structure, although the intensities are not predicted all too well. Interestingly, the predicted intensities for the two band are widely different for the two functionals.

The two calculated vibrational modes correspond to the motion of the two central atoms moving perpendicular to or along the direction of the other two atoms. The calculated spin moment of 2.5 μ_B/atom, which is the same for both isomers and both computational methods, is significantly higher than in the bulk (1.55 μ_B/atom). This is most probably due to the reduced coordination number of 2.5 compared to 12 for the bulk, leading to restricted hybridization of 3d and 4s orbitals. The assignment of the rhombic structure is in agreement with recent calculations on bimetallic cobalt-nickel clusters where also undoped

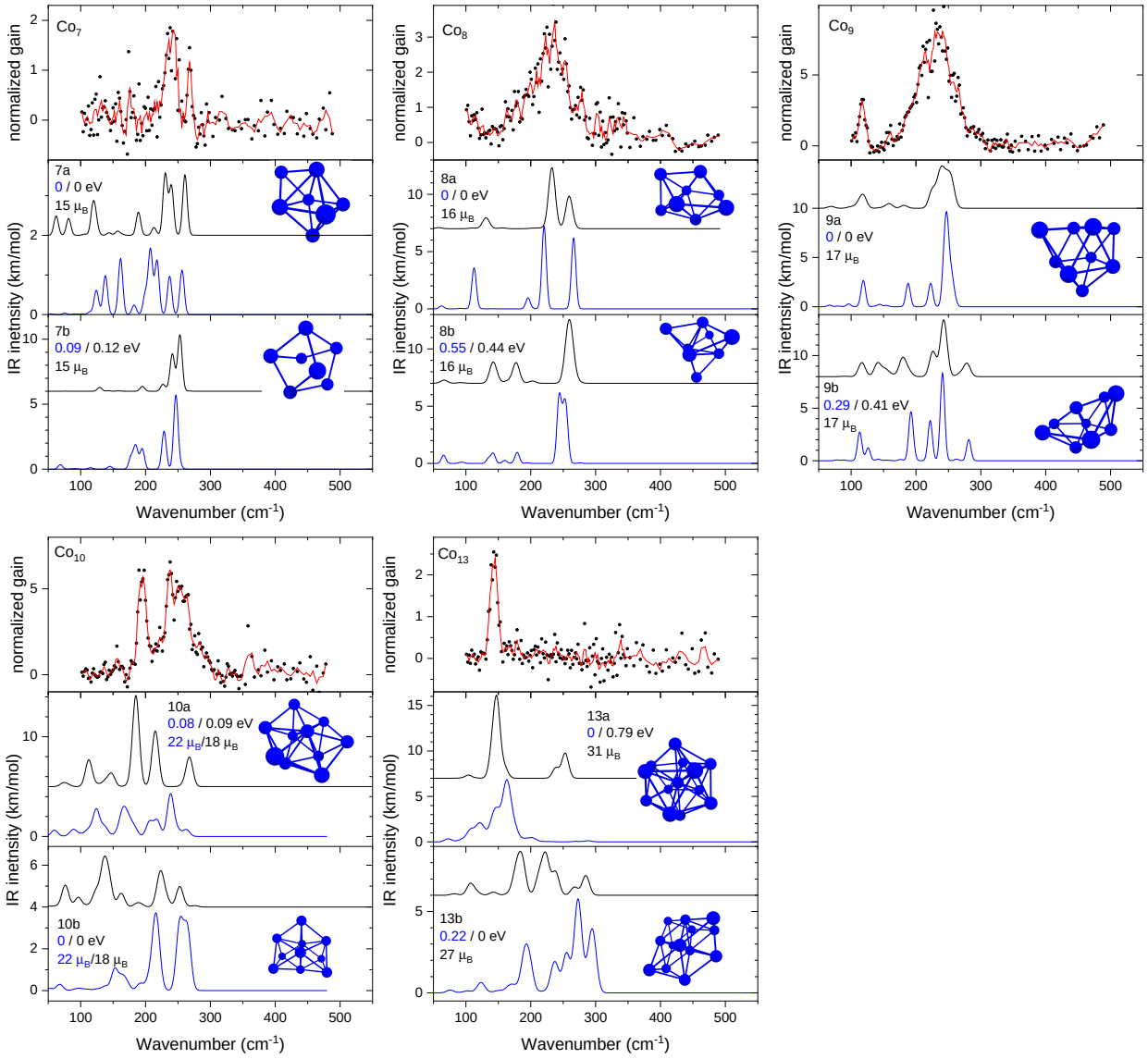

FIG. 3. Experimental vibrational spectra (top panel in each graph) for Co_n, n=7-10,13. Bottom panels: calculated spectra for two isomers for each cluster size with relative energies using the PBE (black) and revTPSS (blue) functionals. The calculated IR intensities (in km/mol) are convoluted with Gaussian lineshape functions with a 15 cm^{-1} width to facilitate comparison with the experimental spectra.

cobalt clusters were studied[30].

The experimental spectra for larger cluster sizes were all recorded using a frequency-tripled dye laser, and are combined in Figure 3. The experimental spectrum for Co_7 reveals one stronger band at 240 cm^{-1} with potentially a second band to the blue at 260 cm^{-1}.

Among reported geometries for Co_7 are a capped octahedron (isomer **7a**)[17] and a pentagonal bipyramid (isomer **7b**)[15]. The cation was found to resemble isomer **7a**[36]. For the neutral Co_7, we do not obtain a conclusive match between experimental and calculated spectrum. Calculated spectra for both isomers exhibit their strongest resonance close to the observed 240 cm^{-1} band. The presence of the 260 cm^{-1} band would suggest that the PBE spectrum for **7a** matches best, but the present data do not make a definitive assignment possible. As the IE of Co_7 is relatively high, 5.98 eV[48], compared to the UV photon energy used to record the vibrational spectra (up to 5.76 eV), we cannot rule out that only the strongest of vibrational bands appear in the current spectrum. The energetics cannot play a decisive role here, either: we deem the found energy difference of 0.1 eV too low to be factored in.

The experimental vibrational spectrum of Co_8 in Figure 3 reveals a clear, rather broad band centered at 231 cm^{-1}, and the appearance of a band at the lower limit of the studied frequency range at 100 cm^{-1}. The 55 cm^{-1} width (FWHM) for the 231 cm^{-1} band suggests the presence of multiple resonances in this spectral range. A bicapped octahedron (isomer **8a**) and a tricapped triangular bipyramid (isomer **8b**) are suggested as candidate structures for Co_8[15–17]. Experimentally, Co_8^+ was found to adopt a structure similar to isomer **8a**[36]. Both functionals used here predict isomer **8a** to be the lowest energy structure by 0.4-0.6 eV. Both structures have a spin magnetic moment of $16\mu_B$. We assign the experimental spectrum to the lowest energy structure, as for both functionals bands are predicted coinciding with the broad resonance, and both predict a smaller resonance at frequencies close to 100 cm^{-1}, where an experimental band surfaces.

The experimental spectrum for Co_9 is dominated by a strong band centered around 225 cm^{-1}, and a smaller yet distinct band at 118 cm^{-1}. The width of the latter of 13cm^{-1} suggests the 225 cm^{-1} band is composed of multiple resonances. A fit using two Gaussian functions provides a band at 202 cm^{-1} and another one at 236 cm^{-1}. Previous computational studies on neutral Co_9 supply two candidate structures, a tricapped octahedron (isomer **9a**),[17] and a bicapped pentagonal bipyramid (isomer **9b**).[15] We find isomer **9a** more stable by 0.3 eV using both methods. The spin magnetic moment of 1.89 μ_B/atom is the same as obtained in previous computational studies. For both isomers several bands are predicted in the range of 100-300 cm^{-1}, and neither structure can be ruled out based on the current data. We lean toward assignment to structure **9a**, both on energetic grounds, and because both functionals predict a rather isolated resonance near 120 cm^{-1}, which matches the

experimental band at 118 cm^{-1}.

The experimental spectrum for Co_{10} reveals two vibrational resonances between 190 and 280 cm^{-1}: the first band is centered at 193 cm^{-1} (FWHM: 18 cm^{-1}); a second, broader, feature is observed around 240 cm^{-1}. The 240 cm^{-1} band is substantially broader, and flattened off. This could either suggest the band is saturated or resulting from multiple bands buried underneath.

We consider a tricapped pentagonal bipyramid **10a** and a tetracapped octahedral isomer, where three of the capping atoms form a second octahedron; the fourth atom bridges the two 'fused' octahedra (**10b**). The DFT calculations indicate that these isomers are competitive: both methods predict **10b** the global minimum, with structure **10b** trailing by only 0.1 eV. Interestingly, both methods predict different spin states for this size: PBE predicts $2S = 18$ for both isomers, while revTPSS comes to $2S = 22$ (see Figure S1 and S2 of the Supporting Information).

The assignment of this spectrum to a specific isomer is difficult. The best match appears to be with structure **10b**, but only at the revTPSS level. The two bands are quite well reproduced here, especially the presence of multiple bands close to 240 cm^{-1}. All other spectra predict significant activity. All in all this is a case where the two functionals show substantial discrepancies, making it difficult to assign the spectrum.

The calculated spin moment of 1.8 μ_B/atom for PBE and 2.2 μ_B/atom for revTPSS is low compared to other clusters in this size range and is significantly lower than the reported magnetic moment of 2.45 μ_B/atom[15]. Datta *et al.*[17] state that this is most likely due to the change in growth pattern from octahedral based structures for smaller clusters and an icosahedral growth pattern for Co_{10}. In our case, we conclude that both functionals still favor an octahedral pattern.

For Co_{13} only one clear resonance is observed at 144 cm^{-1} (FWHM: 14 cm^{-1}). The appearance of only one single band could point at a highly symmetric structure. As 13 is the first cluster size where a geometric shell is closed for both icosahedral and cuboctahedral structures, many computational studies have aimed at finding the geometric arrangement of 13-atom clusters, especially for transition metals. Chang and Chou[61] report a buckled biplanar conformation for 4*d* transition metals using a pseudo-potential DFT method using a GGA functional. Several other groups report a biplanar structure for Co_{13}[29,62,63]. Datta *et al.*[17] indicate that Co_{13} favours a distorted hexagonal structure over an icosahedral

symmetry.

Here, we have calculated the vibrational spectra for an icosahedron and for an fcc-like structure, consisting of a hexagonal and a triangular layer and compared them to the experimental spectrum. We have attempted to also calculate the distorted hexagonal structure proposed by Datta *et al.*[17], but could not suppress imaginary frequencies, indicating that in our approach it should be considered as a saddlepoint, and not a true minimum. The two functionals applied disagree about energetic ordering: PBE prefers the fcc structure by 0.79 eV, whereas revTPSS rates the icosahedron as lowest energy structure, albeit by a mere 0.16 eV. The spin state is predicted the same for both methods, 2S=31 for the icosahedron and 2S=27 for the fcc structure. We assign the experimental spectrum to an icosahedral structure, as it is clear that the rich vibrationla structure predicted for the fcc structure ate higher frequencies is not observed. Interestingly, both theretical spectra for the icosahedron reflect their lowering of symmetry upon geometry optimization, leading to the appearance of (weaker) high frequency band (PBE) or significant broadeing (revTPSS) where the experimental spectrum is rather sharp.

As is clear from the previous, the structure determination of a cluster is not straightforward. For lack of experimental information, computational studies usually assign or compare the geometric structures solely based on the calculated energetic order or the match between calculated and experimental magnetic moment. This can be ambiguous as the calculated moment for different isomers is often identical. Moreover, the experimental magnetic moment is the *total* magnetic moment, whereas the calculations are limited to the *spin* moment alone. From the current calculations we find spin magnetic moments that agree well with with experimental observations, where an increase in total magnetic moment is observed compared to the bulk that increases with reduced cluster size[10]. Additionally, our results are of comparable magnitude to the spin moments determined by XMCD for cobalt cations[19].

Nonetheless, assignment of a cluster structure by comparison of experimental and calculated magnetic moment would be more robust when there is a strong dependence of the magnetic moment on the cluster size. For cobalt clusters, this is not the case. In contrast, the calculated electric dipole moment strongly depends on cluster structure. The electric dipole moment can therefore be considered as an additional experimental probe for the structure. Although the calculated dipole moments differ only negligibly for the two isomers of Co_4 and Co_5, a discrimination based on electric dipole moment is possible for all other

	PBE				revTPSS			
	Relative energy (eV)	Spin state (2S)	Spin magnetic moment (μ_B)	Dipole moment (D)	Relative energy (eV)	Spin state (2S)	Spin magnetic moment (μ_B	Dipole moment (D)
4a	0.13	10	2.50	0.000	0.11	10	2.50	0.000
4b	0.00	10	2.50	0.000	0.00	10	2.50	0.000
5a	0.00	13	2.60	0.000	0.00	13	2.60	0.074
5b	0.14	13	2.60	0.033	0.18	13	2.60	0.058
6a	0[a]	14	2.33	0.330	0.84	14	2.33	0.173
6b	0.00	14	2.33	0.336	0.00	14	2.33	0.000
7a	0.00	15	2.14	0.203	0.00	15	2.14	0.333
7b	0.12	15	2.14	0.107	0.09	15	2.14	0.089
8a	0.00	16	2.00	0.114	0.00	16	2.00	0.013
8b	0.44	16	2.00	0.353	0.55	16	2.00	0.419
9a	0.00	17	1.89	0.234	0.00	17	1.89	0.180
9b	0.41	17	1.89	0.526	0.29	17	1.89	0.651
10a	0.09	18	1.80	1.225	0.08	22	2.20	1.439
10b	0.00	18	1.80	0.180	0.00	22	2.20	0.170
13a	0.79	31	2.38	0.003	0.00	31	2.38	0.003
13b	0.00	27	2.08	0.244	0.22	27	2.08	0.371

TABLE I. Calculated relative energies, spin moment and electronic dipole moment.

[a] Collapses into structure 6b

cluster sizes, as shown in Table I. While electric deflection experiments have, to the best of our knowledge, not been performed for such small cobalt clusters, such data could yield valuable complementary information to the experiments presented here.

V. CONCLUSIONS

We have recorded the vibrational modes for small neutral cobalt clusters (N=4–10,13) via two-color IR-UV spectroscopy. Upon comparison of our experimental data with calculated

spectra using the PBE and revTPSS functionals we tentatively assign the spectra to the following structures: Co_4 is a rhombus, Co_5 a trigonal bipyramid, Co_6 a tetragonal bipyramid, Co_8 a bicapped octahedron, Co_9 a tricapped octahedron, and Co_{13} is found to be an icosahedron. For Co_{10}, we cannot assign the structure as the theoretical spectra simply do not agree with the experimental; we lean to favoring a tricapped pentagonal bipyramid as suggested by the revTPSS calculations. Due to a rather poor signal-to-noise ration, likely caused by a mismatch between UV probe wavelength and IE, the spectrum for Co_7 could not be assigned, either. Our calculations further suggest that experimental determination of the electric dipole moment rather than the magnetic moment could provide additional structural information.

We find that the two functionals used often show strong agreements in predicting the relative stability of structural isomers of the cluster sizes studied. The spin magnetic moments are also usually agreed upon, with the notable exception of Co_{10}, where the methods consistently predict a different lowest energy spin state. However, for predicting the IR spectra of the clusters, we find a substantial variation, making it difficult to assign spectra, even disregarding the usual discrepancies between harmonic frequencies and possible multiple-photon absorption effects. It is with this extensive comparison that we hope to stimulate further development in theoretical treatment of high-spin species, and of transition metal systems in general.

ACKNOWLEDGEMENT

We gratefully acknowledge the Nederlandse Organisatie voor Wetenschappelijk Onderzoek (NWO) for the support of the FELIX Laboratory. We further acknowledge NWO-EW and the SURFsara staff for computational time on the Cartesius computer cluster (grant 16327). We further thank V.J.F. Lapoutre and D. M. Kiawi for assistance during the experiments, A. Fielicke, L. Peters and R. Logemann for stimulating discussions, and B. Sanyal for providing the structures for Co_8–Co_{13}.[17]

REFERENCES

[1]J. V. Barth, G. Costantini, and K. Kern, Nature **437**, 671 (2005).

[2]C. F. Hirjibehedin, C. P. Lutz, and A. J. Heinrich, Science **312**, 1021 (2006).

[3]W. A. de Heer, Rev. Mod. Phys. **65**, 611 (1993).

[4]D. E. Bergeron, P. J. Roach, A. W. Castleman, N. O. Jones, and S. N. Khanna, Science **307**, 231 (2005).

[5]A. W. Castleman, J. Phys. Chem. Lett. **2**, 1062 (2011).

[6]J. Bucher, D. Douglass, and L. Bloomfield, Phys. Rev. Lett **66**, 3052 (1991).

[7]I. M. L. Billas, A. Chatelain, and W. A. de Heer, Science **265**, 1682 (1994).

[8]S. Apsel, J. Emmert, J. Deng, and L. Bloomfield, Phys. Rev. Lett **76**, 1441 (1996).

[9]M. B. Knickelbein, J. Chem. Phys. **125**, 044308 (2006).

[10]F. W. Payne, W. Jiang, J. W. Emmert, J. Deng, and L. A. Bloomfield, Phys. Rev. B **75**, 094431 (2007).

[11]X. Xu, S. Yin, R. Moro, A. Liang, J. Bowlan, and W. A. de Heer, Phys. Rev. Lett **107**, 057203 (2011).

[12]C. Jamorski, A. Martinez, M. Castro, and D. R. Salahub, Phys. Rev. B **55**, 10905 (1997).

[13]M. Castro, C. Jamorski, and D. R. Salahub, Chem. Phys. Lett. **271**, 133 (1997).

[14]M. Pereiro, S. Man'kovsky, D. Baldomir, M. Iglesias, P. Mlynarski, M. Valladares, D. Suarez, M. Castro, and J. E. Arias, Comput. Mater. Sci. **22**, 118 (2001).

[15]J. Rodríguez-López, F. Aguilera-Granja, K. Michaelian, and A. Vega, Phys. Rev. B **67**, 174413 (2003).

[16]Q.-M. Ma, Z. Xie, J. Wang, Y. Liu, and Y.-C. Li, Phys. Lett. A. **358**, 289 (2006).

[17]S. Datta, M. Kabir, S. Ganguly, B. Sanyal, T. Saha-Dasgupta, and A. Mookerjee, Phys. Rev. B **76**, 014429 (2007).

[18]A. Sebetci, Chem. Phys. **354**, 196 (2008).

[19]S. Peredkov, M. Neeb, W. Eberhardt, J. Meyer, M. Tombers, H. Kampschulte, and G. Niedner-Schatteburg, Phys. Rev. Lett **107**, 2 (2011).

[20]M. Niemeyer, K. Hirsch, V. Zamudio-Bayer, A. Langenberg, M. Vogel, M. Kossick, C. Ebrecht, K. Egashira, A. Terasaki, T. Möller, B. von Issendorff, and J. T. Lau, Phys. Rev. Lett **108**, 1 (2012).

[21]A. Langenberg, K. Hirsch, A. Ławicki, V. Zamudio-Bayer, M. Niemeyer, P. Chmiela, B. Langbehn, A. Terasaki, B. von Issendorff, and J. T. Lau, Phys. Rev. B **90**, 184420 (2014).

[22]J. Meyer, M. Tombers, C. Van Wüllen, G. Niedner-Schatteburg, S. Peredkov, W. Eberhardt, M. Neeb, S. Palutke, M. Martins, and W. Wurth, J. Chem. Phys. **143** (2015), 10.1063/1.4929482.

[23]D. Dieleman, M. Tombers, L. Peters, J. Meyer, S. Peredkov, J. Jalink, M. Neeb, W. Eberhardt, T. Rasing, G. Niedner-Schatteburg, and A. Kirilyuk, Phys. Chem. Chem. Phys. **17**, 28372 (2015).

[24]F. A. Reboredo and G. Galli, J. Phys. Chem. B **110**, 7979 (2006).

[25]N. E. Tsakoumis, M. Rønning, Ø. Borg, E. Rytter, and A. Holmen, Catal. Today **154**, 162 (2010).

[26]J. P. D. Breejen, P. B. Radstake, G. L. Bezemer, J. H. Bitter, and V. Frøseth, J. Am. Chem. Soc. , 7197 (2009).

[27]C. D. Zeinalipour-Yazdi and R. A. van Santen, J. Phys. Chem. C **116**, 8721 (2012).

[28]C. P. McNary and P. B. Armentrout, Phys. Chem. Chem. Phys. **16**, 26467 (2014).

[29]F. Aguilera-Granja, A. Vega, and L. C. Balbás, Chem. Phys. **415**, 106 (2013).

[30]P. Parida, A. Kundu, and S. K. Pati, J. Clust. Sci. **20**, 355 (2009).

[31]B. J. Winter, T. D. Klots, E. K. Parks, and S. J. Riley, Z. Phys. D **19**, 375 (1991).

[32]D. Schooss, M. N. Blom, J. H. Parks, B. von Issendorff, H. Haberland, and M. M. Kappes, Nano Lett. **5**, 1972 (2005).

[33]A. Fielicke, G. von Helden, G. Meijer, D. B. Pedersen, B. Simard, and D. M. Rayner, J. Phys. Chem. B **108**, 14591 (2004).

[34]D. G. Leopold and W. C. Lineberger, J. Chem. Phys. **85**, 51 (1986).

[35]H. Yoshida, A. Terasaki, K. Kobayashi, M. Tsukada, and T. Kondow, J. Chem. Phys. **102**, 5960 (1995).

[36]R. Gehrke, P. Gruene, A. Fielicke, G. Meijer, and K. Reuter, J. Chem. Phys. **130**, 034306 (2009).

[37]M. Putter, G. von Helden, and G. Meijer, Chem. Phys. Lett. **258**, 118 (1996).

[38]T. Omi, H. Shitomi, N. Sekiya, K. Takazawa, and M. Fujii, Chem. Phys. Lett. **252**, 287 (1996).

[39]C. Steinbach and U. Buck, J. Chem. Phys. A **110**, 3128 (2006).

[40]A. Fielicke, J. T. Lyon, M. Haertelt, G. Meijer, P. Claes, J. de Haeck, and P. Lievens, J. Chem. Phys. **131**, 171105 (2009).

[41]M. Haertelt, A. Fielicke, G. Meijer, K. Kwapien, M. Sierka, and J. Sauer, Phys. Chem. Chem. Phys. **14**, 2849 (2012).

[42]C. Romanescu, D. J. Harding, A. Fielicke, and L.-S. Wang, J. Chem. Phys. **137**, 014317 (2012).

[43]J. Jalink, J. M. Bakker, T. Rasing, and A. Kirilyuk, J. Phys. Chem. Lett. **6**, 750 (2015).

[44]J. M. Bakker, V. J. F. Lapoutre, B. Redlich, J. Oomens, B. G. Sartakov, A. Fielicke, G. von Helden, G. Meijer, and A. F. G. van der Meer, J. Chem. Phys. **132**, 074305 (2010).

[45]M. Haertelt, V. J. F. Lapoutre, J. M. Bakker, B. Redlich, D. J. Harding, and G. Meijer, J. Chem. Phys. Lett. **2**, 1720 (2011).

[46]S. Ishiuchi, H. Shitomi, K. Takazawa, and M. Fujii, Chem. Phys. Lett. , 243 (1998).

[47]E. K. Parks, T. D. Klots, and S. J. Riley, J. Chem. Phys. **92**, 3813 (1990).

[48]S. Yang and M. B. Knickelbein, J. Chem. Phys. **93**, 1533 (1990).

[49]C. Fonseca Guerra, J. G. Snijders, G. te Velde, and E. J. Baerends, Theor. Chim. Acta **99**, 391 (1998).

[50]G. te Velde, F. M. Bickelhaupt, E. J. Baerends, C. Fonseca Guerra, S. J. A. van Gisbergen, J. G. Snijders, and T. Ziegler, J. Comput. Chem. **22**, 931 (2001).

[51]E. J. Baerends, T. Ziegler, A. J. Atkins, J. Autschbach, D. Bashford, A. Bérces, F. M. Bickelhaupt, C. Bo, P. M. Boerritger, L. Cavallo, D. P. Chong, D. V. Chulhai, L. Deng, R. M. Dickson, J. M. Dieterich, D. E. Ellis, M. van Faassen, A. Ghysels, A. Giammona, S. J. A. van Gisbergen, A. W. Götz, S. Gusarov, F. E. Harris, P. van den Hoek, C. R. Jacob, H. Jacobsen, L. Jensen, J. W. Kaminski, G. van Kessel, F. Kootstra, A. Kovalenko, M. Krykunov, E. van Lenthe, D. A. McCormack, A. Michalak, M. Mitoraj, S. M. Morton, J. Neugebauer, V. P. Nicu, L. Noodleman, V. P. Osinga, S. Patchkovskii, M. Pavanello, C. A. Peeples, P. H. T. Philipsen, D. Post, C. C. Pye, W. Ravenek, J. I. Rodríguez, P. Ros, R. Rüger, P. R. T. Schipper, H. van Schoot, G. Schreckenbach, J. S. Seldenthuis, M. Seth, J. G. Snijders, M. Solà, M. Swart, D. Swerhone, G. te Velde, P. Vernooijs, L. Versluis, L. Visscher, O. Visser, F. Wang, T. A. Wesolowski, E. M. van Wezenbeek, G. Wiesenekker, S. K. Wolff, T. K. Woo, and A. L. Yakovlev, "ADF2016, SCM, Theoretical Chemistry, Vrije Universiteit, Amsterdam, The Netherlands, https://www.scm.com,".

[52]J. Perdew, K. Burke, and M. Ernzerhof, Phys. Rev. Lett **77**, 3865 (1996).

[53]S. Datta, M. Kabir, and T. Saha-Dasgupta, Phys. Rev. B **84**, 1 (2011).

[54]J. Tao, J. Perdew, V. Staroverov, and G. Scuseria, Phys. Rev. Lett **91**, 3 (2003).

[55]J. P. Perdew, A. Ruzsinszky, G. I. Csonka, L. A. Constantin, and J. Sun, Phys. Rev. Lett **103**, 026403 (2009).

[56]M. Johansson, A. Lechtken, D. Schooss, M. Kappes, and F. Furche, Phys. Rev. A **77**, 053202 (2008).

[57]A. Fielicke, P. Gruene, M. Haertelt, D. J. Harding, and G. Meijer, J. Phys. Chem. A **114**, 9755 (2010).

[58]M. D. Halls, J. Velkovski, and H. B. Schlegel, Theor Chem Acc **105**, 413 (2001).

[59]V. Barone, J. Chem. Phys. **122**, 014108 (2005).

[60]R. Lindner, K. Müller-Dethlefs, E. Wedum, K. Haber, and E. R. Grant, Science **271**, 1698 (1996).

[61]C. Chang and M. Chou, Phys. Rev. Lett **93**, 133401 (2004).

[62]M. J. Piotrowski and P. Piquini, Phys. Rev. B **81**, 155446 (2010).

[63]K. García-Díez, J. Fernández-Fernández, J. A. Alonso, and M. J. López, Phys. Chem. Chem. Phys. **20**, 21163 (2018).

SUPPORTING INFORMATION

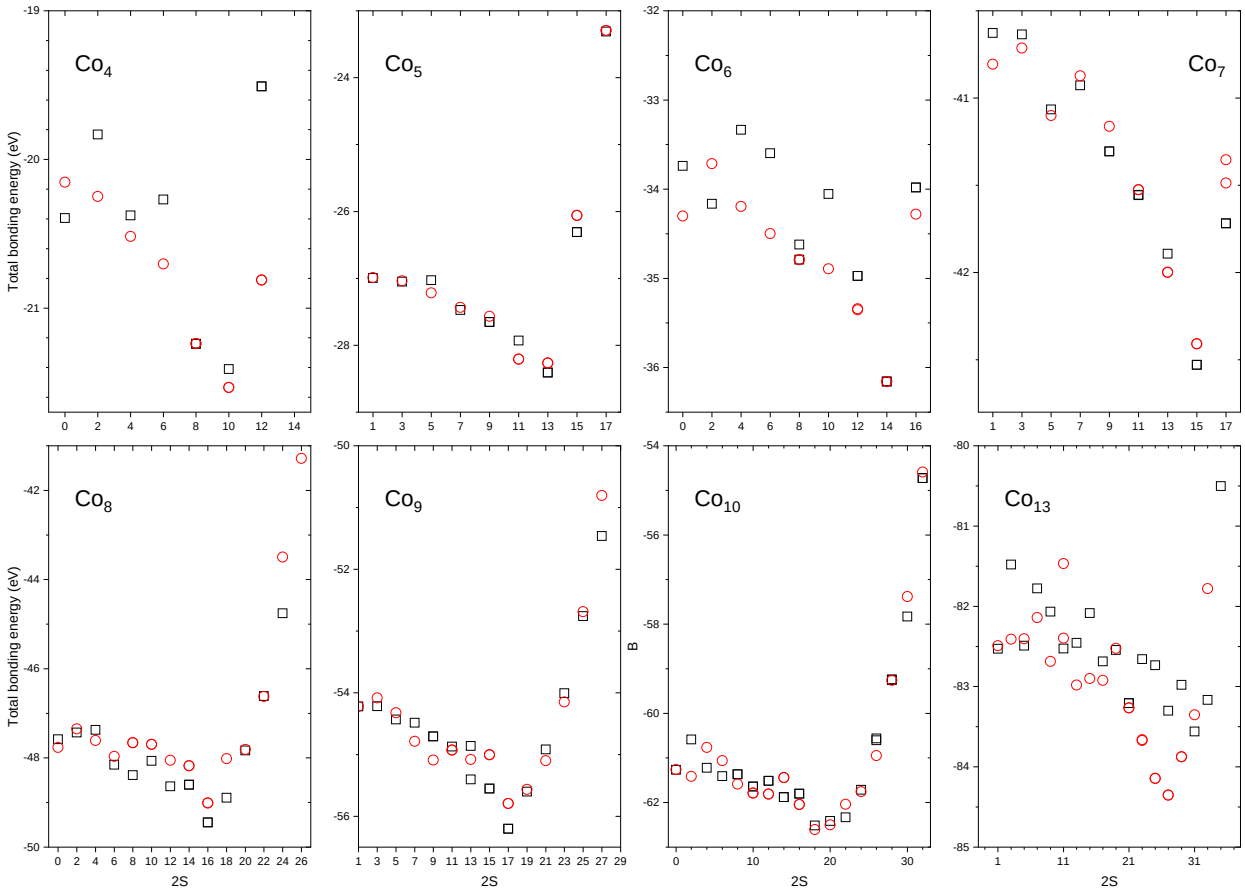

FIG. S1. Total bonding energy including zero point energy of the Co_n cluster structures as a function of spin state calculated using the PBE functional. Structures ***n*a** are shown in black squares, structures ***n*b** in red circles.

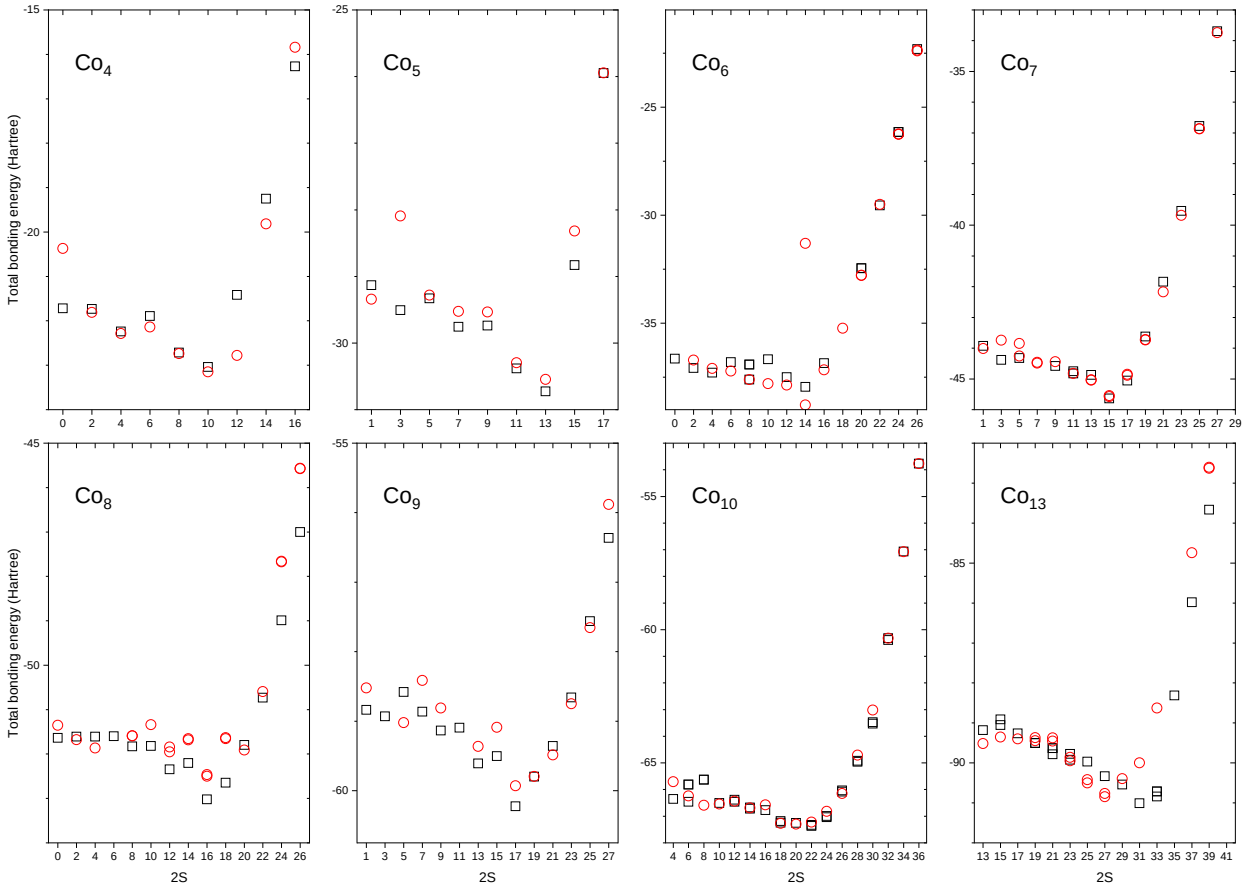

FIG. S2. Total bonding energy including zero point energy of the Co_n cluster structures as a function of spin state calculated using the revTPSS functional. Structures $\boldsymbol{n}$**a** are shown in black squares, structures $\boldsymbol{n}$**b** in red circles.

4a	0	-1.68036	-8E-08
	0	6.85E-05	-1.33555
	0	6.84E-05	1.33555
	0	1.680224	-1.1E-07
4b	-0.96588	0.965823	-0.462
	0.965784	-0.96587	-0.46218
	0.966056	0.966016	0.461905
	-0.96595	-0.96597	0.462278
5a-pbe	1.40704	1.057068	1.567581
	2.300266	-0.18685	4.52E-05
	-0.11343	0.902119	-2.4E-05
	1.407006	1.057136	-1.56756
	2.039863	2.449351	-4.1E-05
5a-tpss	1.403421	1.081053	1.562916
	2.280129	-0.17904	0.000278
	-0.08318	0.881865	-0.00015
	1.403143	1.081305	-1.56299
	2.037237	2.413641	-5.6E-05
5b	-5.9E-05	5.42E-05	1.691566
	-1.08834	1.088341	-0.09785
	-1.08822	-1.08837	-0.09789
	1.088369	1.088225	-0.09789
	1.088253	-1.08825	-0.09794
6a-tpss	0.039278	1.098899	1.30179
	-1.22898	0.318197	-0.43986
	0.522247	1.709318	-0.77363
	1.228911	-0.31821	-0.43992
	-0.52216	-1.70933	-0.77364
	-0.0393	-1.09887	1.301786
6b	1.915192	-0.38115	-0.00065
	1.803396	1.223159	1.607046
	3.406548	1.335352	-0.00038
	1.802843	1.223076	-1.60532
	0.20207	1.111079	1.48E-05
	1.690627	2.827373	-0.00068
7a	-0.39707	1.282558	0.071481
	-0.2249	-1.93407	-0.0964
	0.794403	-0.19749	-1.18162
	-1.47376	-0.33037	-1.15338
	0.821546	-0.31751	1.142694
	-1.44702	-0.45164	1.139155
	1.920881	1.398795	0.060396
7b	1.793098	-0.02402	0.046565
	0.608232	1.856096	0.023482
	-1.47941	1.168389	0.034643
	-1.53921	-1.02653	0.060879
	0.505292	-1.83337	0.069779
	0.000912	0.045707	1.470092
	-0.00366	0.010409	-1.37509
8a	1.486975	0.020077	0.538155
	-1.45576	-0.01881	0.384525
	0.047664	1.435648	-0.5107
	-0.07199	1.198358	1.785991
	0.080449	-1.50943	-0.38758
	-0.04213	-1.0805	1.88198
	1.277613	-0.07679	-1.76354
	-1.00135	-0.11029	-1.88037
8b	0.776314	-0.80096	-0.81112
	0.809557	0.837443	0.900103
	-0.88116	-0.82138	0.839858
	-0.93741	0.845984	-0.85351
	1.294404	-1.30768	1.360495
	1.209129	1.395336	-1.24826
	-1.39617	-1.29299	-1.34061
	-1.34672	1.363515	1.297266
9a	-0.11912	-0.04594	-2.30757
	1.058396	1.144899	-0.69022
	-1.10511	0.000273	1.323932
	-1.1695	-1.20423	-0.58397
	0.007816	-2.04862	1.239118
	1.061023	-1.19708	-0.66273
	-1.17162	1.15236	-0.61534
	1.133339	-0.00061	1.253058
	0.005056	2.051005	1.187775
9b	1.588204	0.02608	0.354622
	0.214427	1.926708	0.402076
	-2.02928	1.149936	0.523827
	-1.99283	-1.20547	0.558758
	0.275022	-1.91536	0.457436
	-0.36259	0.013807	1.631607
	-0.50657	-0.02372	-0.71899
	1.228867	1.170789	-1.61083
	1.267905	-1.18575	-1.57632
10a	-1.11633	2.002228	-0.86259
	1.128687	1.966128	-0.05025
	0.040742	0.032999	-0.7502
	-0.6984	1.176571	1.194807
	-2.20871	-0.00186	-0.16038
	-1.07772	-1.95003	-0.95446
	2.323102	0.056855	-0.84386
	-0.67553	-1.21216	1.139331
	1.165655	-1.90876	-0.13878
	1.380941	0.000958	1.207074
10b	-2.02253	-1.21212	-0.86779
	1.789368	-1.1082	-0.92771
	-2.07619	1.056512	-0.97896
	1.722945	1.179531	-1.02644
	-0.14597	-0.04834	-1.57297
	-1.97098	0.019814	1.076439
	1.831289	0.126766	1.011704
	-0.08875	-1.13156	0.460084
	-0.14787	1.206313	0.364149
	-0.00573	0.115908	2.429775
13a	0.064536	-0.03164	0.019099
	0.001495	-0.11152	2.339695
	0.131649	0.054808	-2.30069
	1.75836	1.219525	-0.95257
	-0.55679	1.974585	-0.96653
	-2.00131	0.011756	-1.04133
	-0.54507	-1.98551	-1.07405
	1.768255	-1.2164	-1.01828
	0.670784	1.924765	1.112579
	-1.63932	1.155958	1.054376
	-1.62998	-1.277	0.996588
	0.683717	-2.03841	1.003514
	2.129978	-0.07888	1.07829
13b	-1.38866	0.006847	1.002684
	0.690954	1.210819	1.016514
	-1.36843	2.367943	1.027769
	-1.36293	-2.35371	0.97168
	0.693667	-1.19302	0.987667
	2.725978	0.011344	0.996393
	-0.00256	0.031298	-0.91668
	2.083458	1.202993	-0.8137
	-0.03714	2.423431	-0.79805
	-2.06214	1.251145	-0.81126
	-2.05896	-1.19536	-0.84061
	-0.03173	-2.36336	-0.85531
	2.086075	-1.13743	-0.84198

FIG. S3. Coordinates (in Å) of the Co_n cluster structures optimized at the PBE level (unless otherwise indicated) for the lowest found spin state.